

Gradient-Based Predictive Pulse Pattern Control with Active Neutral Point Balancing for Three-Level Inverter Medium-Voltage Drives

Mirza Abdul Waris Begh*, Petros Karamanakos*, and Tobias Geyer†

*Faculty of Information Technology and Communication Sciences, Tampere University, Tampere, Finland,

†ABB System Drives, Turgi, Switzerland

Email: *mirza.begh@tuni.fi, *p.karamanakos@ieee.org, †t.geyer@ieee.org

Abstract—This paper presents a control method for three-level neutral point clamped (NPC) inverter medium-voltage (MV) drives that addresses the stator current control problem and balancing of the neutral point (NP) potential in a single control loop. To do so, a model predictive control (MPC) algorithm, designed as a multiple-input multiple-output (MIMO) controller, manipulates optimized pulse patterns (OPPs) in real time. As a result, minimal current harmonic distortions are produced, while the NP potential is kept balanced both during steady state and transients. The presented results demonstrate the effectiveness of the proposed control strategy for three-level NPC inverter MV variable speed drive systems.

Index Terms—Medium-voltage (MV) drives, model predictive control (MPC), optimized pulse patterns (OPPs), reference trajectory tracking, optimal control, pulse width modulation (PWM).

I. INTRODUCTION

Multilevel converters are widely used in industrial applications to drive medium-voltage (MV) machines. To operate MV drives with high efficiency, operation at very low switching frequencies is required to minimize the switching power losses [1]. However, such low switching frequencies can lead to high current distortions, and thus adverse effects, such as increased losses in the machine. To address this issue, optimized pulse patterns (OPPs) can be employed as they are computed to produce the theoretical minimum current distortions [2].

Control of OPPs, however, is a nontrivial task. This is due to the fact that OPPs do not have a fixed-length modulation interval, meaning that when sampling occurs, not only the fundamental component is sampled, but also the ripple. Moreover, the discontinuities in the switching angles with respect to the modulation index complicates the controller design. As a result, OPPs have been traditionally used with low-bandwidth controllers. Alas, such controllers cannot achieve satisfactory transient performance and disturbance rejection.

To address the above, high-bandwidth controllers that adopt the concept of trajectory tracking control have been proposed to manipulate OPPs in real time. For example, control methods based on deadbeat control principles were proposed in [3]–[5]. While the control scheme in [3], [4] is based on the concept of stator *current* trajectory tracking, the control scheme in [5] utilizes the stator *flux* trajectory. A more evolved controller designed in the framework of model predictive control (MPC)—

known as model predictive pulse pattern control (MP³C)—was presented in [6]. This method manipulates OPPs in real time and has been validated experimentally in industrial MV drive systems [7], [8]. In particular, MPC with OPPs is an attractive option since it can take advantage of the excellent steady-state performance and low current harmonic distortions attributed to OPPs as well as the fast dynamic responses that can be achieved with MPC. In this direction, the control method named gradient-based predictive pulse pattern control (GP³C) was recently proposed [9] to achieve superior steady-state and dynamic performance for drive systems. The GP³C method tracks the optimal stator current reference by *optimally* modifying the switching time instants of the nominal OPP.

Nevertheless, the above-mentioned control techniques need to meet additional control objectives when multilevel converters are considered as their internal voltages need to be balanced during the whole operation of the system. For example, when neutral point clamped (NPC) inverters are of interest, the neutral point (NP) potential should be kept around zero to avoid deviations of the phase voltages from the expected voltage levels. Hence, even though the NPC inverter has an inherent natural balancing mechanism [10], active balancing techniques are commonly employed to prevent the NP potential from drifting away.

To this aim, a variety of control strategies have been used to tackle the problem of NP potential balancing. Most of these methods are based on the manipulation of the common-mode component of the output voltage [11]–[13]. Therefore, control of the NP potential is achieved by using an outer loop to manipulate the common-mode component of the reference voltage that is fed to the modulator. Alternatively, control of the NP potential can be achieved by exploiting the redundant switching vectors of the NPC inverter [14]. It should be noted, however, that the effectiveness of these methods diminishes as the phase between the inverter voltage and current approaches 90° [13].

Addition of external loops, however, can further limit the controller bandwidth. For this reason, the developed closed-loop control methods that manipulate OPPs aim at incorporating the NP potential balancing mechanism into the inner control loop. In this direction, similar to [14], [15] adopts the concept of redundant vector manipulation. By selecting appro-

appropriate redundant sub-bridges during steady-state and transient operation, the control method eliminates the NP potential error at low modulation indices while operating the power converter at low switching frequencies. In [16], a push-pull configuration for a variable-speed drive is presented where a five-level OPP is mapped into two three-level OPPs for two NPC inverters. This gives rise to an additional degree of freedom which can be utilized to balance the NP potential. In [17], the MP³C method addresses the balancing of the NP potential by adding an extra term to the objective function to penalize the deviation of the dc component of the NP potential from its reference. Nevertheless, during the derivation of the control problem, a number of assumptions are made that can compromise the overall performance of the control scheme. As a result, the controller design becomes more complicated.

Motivated by the above, this work refines the GP³C method to tackle the problem of the NP potential balancing in a simple, yet effective, manner. By exploiting the high design versatility of GP³C, attributed to its modeling principle, i.e., the use of the gradient of the system output to predict its evolution, the current control and NP potential balancing problems are tackled in one computational stage. In doing so, unlike traditional balancing methods, the proposed method does not rely on manipulating the common-mode voltage of the inverter, but it rather directly regulates the (instantaneous) NP potential along its reference.¹ This equips the GP³C method with a high bandwidth and a high degree of disturbance rejection. The efficacy of the proposed method is demonstrated with an MV drive system consisting of a three-level NPC inverter and an induction machine (IM).

II. MODEL OF THE MV DRIVE SYSTEM

Consider the MV variable speed drive system consisting of a three-level NPC voltage source inverter and an IM, as shown in Fig. 1. The mathematical model of the system is derived in the stationary $\alpha\beta$ -frame, where the transformation matrix

$$\mathbf{K} = \frac{2}{3} \begin{bmatrix} 1 & -\frac{1}{2} & -\frac{1}{2} \\ 0 & \frac{\sqrt{3}}{2} & -\frac{\sqrt{3}}{2} \end{bmatrix}, \quad (1)$$

is used to transform the three-phase quantities into the $\alpha\beta$ -frame. Throughout this paper, the quantities are normalized and presented in the per unit (p.u.) system.

The dc link of the inverter comprises two identical capacitors C_{dc} with (inverse) reactance X_{dc} ; the midpoint N is the so-called neutral point (NP). The total (instantaneous) dc-link voltage is $v_{dc} = v_{dc,up} + v_{dc,lo}$, where $v_{dc,up}$ and $v_{dc,lo}$ denote the upper and the lower dc-link capacitor voltages, respectively. Depending on the *single-phase* switch position $u_x \in \{-1, 0, 1\}$ in phase $x \in \{a, b, c\}$ the inverter can produce three possible phase voltage levels, namely $v_{dc,lo}$, 0, and $v_{dc,up}$, respectively. Hence, the three-phase output voltage of the inverter in the $\alpha\beta$ -frame is a function of the *three-phase* switch position $\mathbf{u}_{abc} = [u_a \ u_b \ u_c]^T$, and it is given by

$$\mathbf{v}_s = \frac{v_{dc}}{2} \mathbf{K} \mathbf{u}_{abc} - v_n \mathbf{K} |\mathbf{u}_{abc}|, \quad (2)$$

¹It should be noted that the proposed control method does not aim to reduce the ripple of the NP potential during steady-state operation, as this is a natural characteristic of the NP potential v_n .

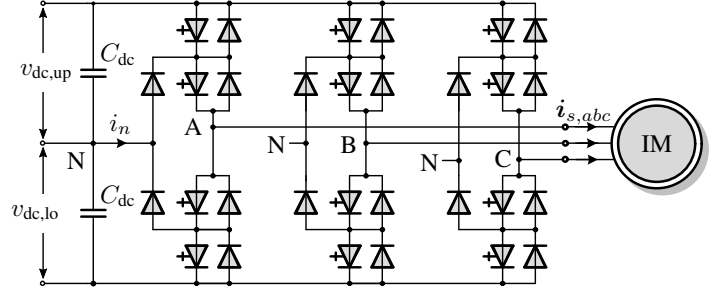


Fig. 1: Three-level neutral point clamped (NPC) voltage source inverter driving an induction machine.

where $|\mathbf{u}_{abc}| = [|u_a| \ |u_b| \ |u_c|]^T$ is the component-wise absolute value of the three-phase switch position. Note that since the inverter is driving a machine, the output voltage of the inverter is equal to the stator voltage \mathbf{v}_s .

As can be seen in (2), the output inverter voltage fluctuates with the NP potential, defined as

$$v_n = \frac{1}{2}(v_{dc,lo} - v_{dc,up}).$$

This potential evolves as a function of the current flowing through the NP [18], i.e.,

$$\frac{dv_n}{dt} = \frac{1}{2} \left(\frac{dv_{dc,lo}}{dt} - \frac{dv_{dc,up}}{dt} \right) = -\frac{1}{2X_{dc}} i_n. \quad (3)$$

The NP current i_n changes when a phase current i_{sx} flows through the NP. This happens when the corresponding switch position u_x is zero, meaning that i_n is a function of \mathbf{u}_{abc} and the inverter (i.e., stator) current $\mathbf{i}_{s,abc} = [i_{sa} \ i_{sb} \ i_{sc}]^T$ according to

$$i_n = (1-|u_a|)i_{sa} + (1-|u_b|)i_{sb} + (1-|u_c|)i_{sc} = -|\mathbf{u}_{abc}|^T \mathbf{i}_{abc}, \quad (4)$$

where a star connection for the load is assumed, i.e., $i_{sa} + i_{sb} + i_{sc} = 0$. Using (3) and (4), the evolution of the NP potential can be written as

$$\frac{dv_n}{dt} = \frac{1}{2X_{dc}} |\mathbf{u}_{abc}|^T \mathbf{i}_{abc}. \quad (5)$$

Regarding the dynamics of the squirrel cage IM in Fig. 1, these can be described by the differential equations of the stator current \mathbf{i}_s and the rotor flux ψ_r ,² i.e., [19]

$$\frac{d\mathbf{i}_s}{dt} = -\frac{1}{\tau_s} \mathbf{i}_s + \left(\frac{1}{\tau_r} \mathbf{I}_2 - \omega_r \begin{bmatrix} 0 & -1 \\ 1 & 0 \end{bmatrix} \right) \frac{X_m}{D} \psi_r + \frac{X_r}{D} \mathbf{v}_s, \quad (6a)$$

$$\frac{d\psi_r}{dt} = \frac{X_m}{\tau_r} \mathbf{i}_s - \frac{1}{\tau_r} \psi_r + \omega_r \begin{bmatrix} 0 & -1 \\ 1 & 0 \end{bmatrix} \psi_r. \quad (6b)$$

In (6), R_s and R_r are the stator and rotor resistance, respectively, while X_{ls} , X_{lr} , and X_m are the stator leakage, rotor leakage, and mutual reactance, respectively. Moreover, $\tau_s = X_r D / (R_s X_r^2 + R_r X_m^2)$ and $\tau_r = X_r / R_r$ are the transient stator and the rotor time constants, respectively, while the constant D is defined as $D = X_s X_r - X_m^2$, with $X_s = X_{ls} + X_m$ and $X_r = X_{lr} + X_m$. In addition, ω_r is the

²Note that the mechanical dynamics are neglected in the subsequent modeling—and the prediction model—as they are slower than the electrical dynamics.

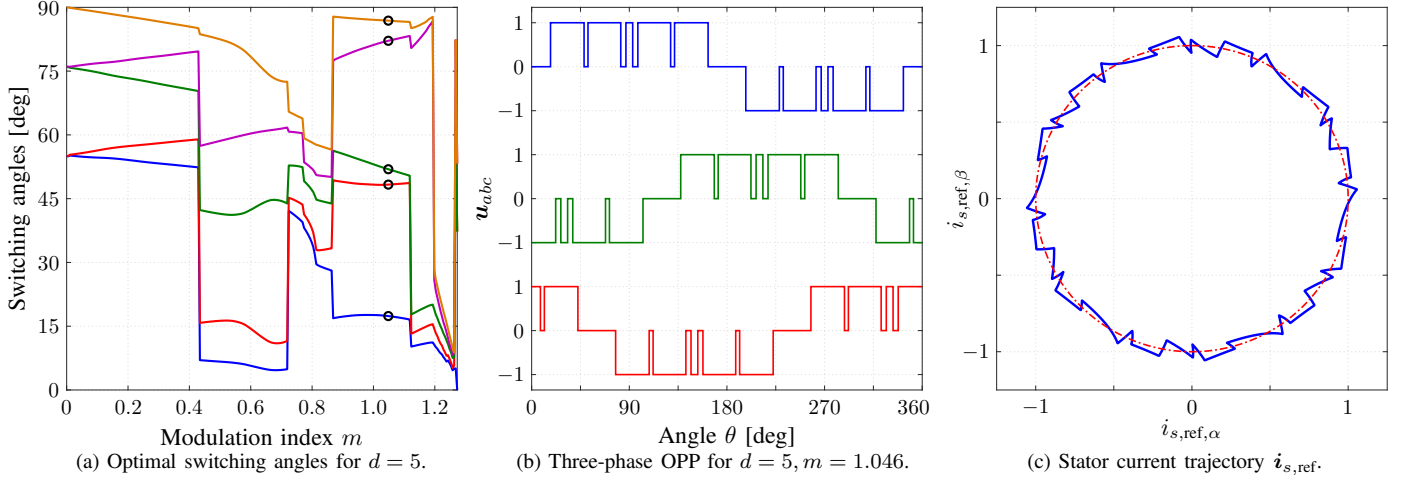


Fig. 3: (a) OPP $p(d, m)$ for a three-level converter with $d=5$ switching angles per quarter of the fundamental period. The optimal switching angles for the modulation index $m=1.046$ are indicated by (black) circles. (b) Three-phase OPP for $m=1.046$. (c) The current reference trajectory (solid blue line) for the given three-phase OPP is a combination of the fundamental component $i_{s1,ref}$ (red dash-dotted line) and the harmonic component $i_{sh,ref}$.

between the output tracking and allowed modifications in the nominal OPP.

Function (10) needs to be minimized to obtain the vector of modified switching time instants t . To do so, the evolution of the output variables within the prediction horizon must be computed. As the OPP switch positions u_{abc} that fall within T_p are known, see the switching sequences U (9b), the evolution of the system output can be computed based on its gradient. Specifically, it can be assumed that the output evolves with a constant gradient within each subinterval $\Delta t_{\ell,ref}$, where

$$\Delta t_{\ell,ref} = t_{\ell+1,ref} - t_{\ell,ref}, \quad (11)$$

and $\ell \in \{0, 1, 2, \dots, z-1\}$. As a result, the output trajectories can be described by their associated gradients, i.e.,

$$m(t_{\ell,ref}) = \frac{y(t_{\ell+1,ref}) - y(t_{\ell,ref})}{\Delta t_{\ell,ref}} = C \frac{x(t_{\ell+1,ref}) - x(t_{\ell,ref})}{\Delta t_{\ell,ref}}. \quad (12)$$

Note that in (12), the gradients at the nominal OPP switching instants $t_{1,ref}, t_{2,ref}, \dots, t_{z,ref}$ are dependent on the predicted state, i.e., $x(t_{1,ref}), x(t_{2,ref}), \dots, x(t_{z,ref})$, respectively, to provide the most accurate computation of the corresponding gradient. This is accomplished by employing the discrete-time system model (8).

Finally, based on the above expressions and by introducing some assumptions as outlined in [9], the objective function (10) is rewritten as

$$J = \|r - Mt\|_Q^2 + \lambda_t \|\Delta t\|_2^2, \quad (13)$$

where r is a vector that depends on the reference values and measurements of the outputs, and M is a matrix of the slopes with which the controlled variables evolve over the prediction horizon, see Appendix B.

C. Control Algorithm

The proposed control method is designed in the discrete-time domain and works at equally spaced time instants kT_s .

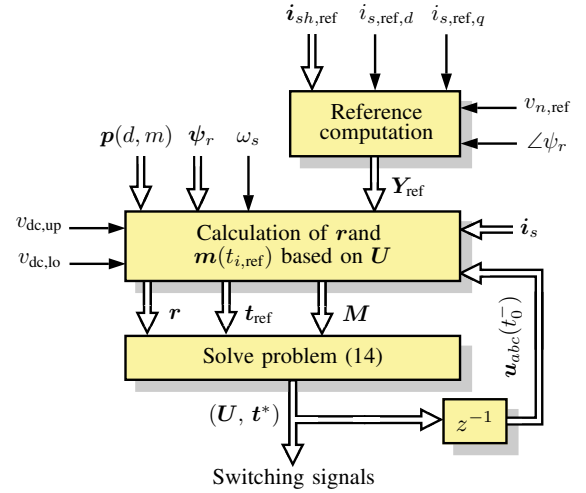


Fig. 4: Inner control loops of the GP3C algorithm.

Algorithm 1: Gradient-based predictive pulse pattern control

- Given $u_{abc}(t_0)$, $x(t_0)$, $i_{s,ref,dq}$, $v_{n,ref}$ and $p(d, m)$
1. Extract the z switching time instants and switch positions that fall within T_p from the nominal OPP $p(d, m)$ to formulate t_{ref} and U .
 2. Compute the reference values of outputs $y_{ref}(t_{i,ref})$, $i \in \{1, 2, \dots, z\}$.
 3. Formulate the gradients $m(t_{\ell,ref})$, $\ell \in \{0, 1, 2, \dots, z-1\}$.
 4. Solve the optimization problem (14). This yields t^* .
- Return $t^*(k)$ that fall within T_s and modify the OPP accordingly.

The block diagram of the inner control loop is shown in Fig. 4. Furthermore, Algorithm 1 provides the pseudocode of the proposed control method.

Before the control algorithm is executed, the offline computed nominal OPP and harmonic current references are retrieved from the look-up tables (LUTs) where they are stored. With this, the three-phase OPP is computed and the stator current reference over the prediction horizon is constructed. Fol-

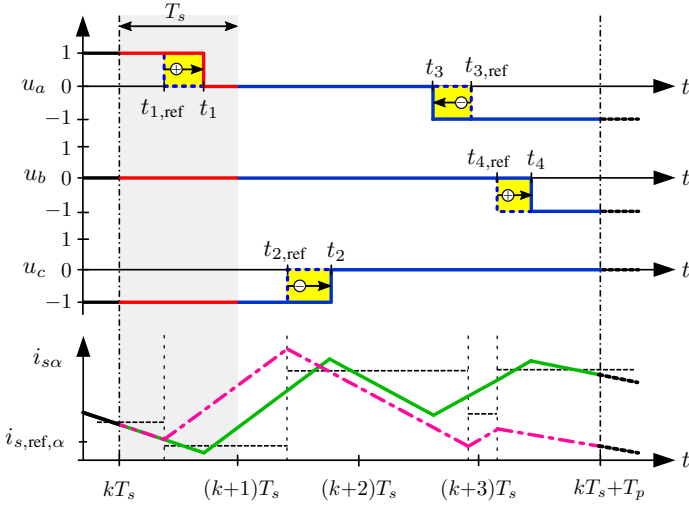


Fig. 5: Example of trajectory tracking of GP³C for one of the controlled variables (e.g., stator current $i_{s\alpha}$) within a four-step ($T_p = 4T_s$) prediction horizon. The nominal OPP instants $t_{i,\text{ref}}$ (dotted line) and the modified switching instants t_i (solid line) are shown, where $i \in \{1, 2, 3, 4\}$. The modifications introduced by the controller are highlighted in yellow. In the bottom figure, the dash-dotted (magenta) line represents the current trajectory when applying the nominal OPP, while the solid (green) line shows the current trajectory based on the modified pulse pattern. The dashed (black) line is the current reference sampled at the nominal OPP time instants.

lowing, the current reference is aggregated into the output reference vector $\mathbf{Y}_{\text{ref}} = [\mathbf{y}_{\text{ref}}^T(t_{1,\text{ref}}) \quad \mathbf{y}_{\text{ref}}^T(t_{2,\text{ref}}) \quad \dots \quad \mathbf{y}_{\text{ref}}^T(t_{z,\text{ref}})]^T$. In a next step, according to (12), z unique output vector gradients are computed within the subintervals of the prediction horizon using the nominal OPP switching instants and the corresponding predicted output variables. This yields the gradient matrix \mathbf{M} . Finally, the modified switching instants $\mathbf{t}^* = [t_1^* \quad t_2^* \quad \dots \quad t_z^*]^T$ are computed by solving the optimization problem

$$\begin{aligned} & \underset{\mathbf{t} \in \mathbb{R}^z}{\text{minimize}} && \|\mathbf{r} - \mathbf{M}\mathbf{t}\|_{\mathbf{Q}}^2 + \lambda_t \|\Delta\mathbf{t}\|_2^2 \\ & \text{subject to} && kT_s < t_1 < \dots < t_z < kT_s + T_p. \end{aligned} \quad (14)$$

As per the receding horizon policy, the switch positions that fall within the first sampling interval T_s are implemented at the corresponding time instants \mathbf{t}^* .⁶

For a better understanding, the following example is provided.

Example 1: Consider the drive system in Fig. 1. As depicted in Fig. 5, $\mathbf{u}_{abc}(t_0^-) = [1 \ 0 \ -1]^T$, with $t_0 \equiv kT_s$, is the three-phase switch position applied at the end of the previous sampling interval. According to the illustrated OPP, four nominal switching time instants $t_{1,\text{ref}}, t_{2,\text{ref}}, t_{3,\text{ref}}$, and $t_{4,\text{ref}}$, with switch positions $\mathbf{u}_{abc}(t_{1,\text{ref}})$, $\mathbf{u}_{abc}(t_{2,\text{ref}})$, $\mathbf{u}_{abc}(t_{3,\text{ref}})$, and $\mathbf{u}_{abc}(t_{4,\text{ref}})$, respectively, fall within the prediction horizon T_p . These instants divide the horizon into five subintervals. Within each subinterval, it is assumed that the system output evolves with a constant gradient. Therefore, with the help of the discrete-time model (8) the evolution of the output can be predicted based on the corresponding gradients $\mathbf{m}(t_{\ell,\text{ref}})$. For example, evolution of one of the controlled variables, i.e., $i_{s\alpha}$ (dash-dotted, magenta line), is shown in Fig. 5 along with its

⁶For more details on the operation of the control algorithm, the reader is referred to [9].

Table I: Rated values (left) and parameters (right) of the drive.

Induction motor	Voltage	3300 V	R_s	0.0108 p.u.
	Current	356 A	R_r	0.0091 p.u.
	Real power	1.646 MW	X_{ls}	0.1493 p.u.
	Apparent power	2.034 MVA	X_{lr}	0.1104 p.u.
	Stator frequency	$2\pi 50$ rad/s	X_m	2.3489 p.u.
	Rotational speed	596 rpm		
	Torque	26.2 kNm		
Inverter	Dc-link voltage	5200 V	V_{dc}	1.9299 p.u.
	Dc-link capacitance	2.24 mF	X_{dc}	3.7628 p.u.

sampled reference (dashed, black line). With the knowledge of the evolution of the system output within the horizon T_p , the GP³C algorithm manipulates the OPP such that the error between the output and its reference is minimized, e.g., the error between $i_{s\alpha}$ and $i_{s,\text{ref},\alpha}$ in Fig. 5. In doing so, the modified switching instants t_1 – t_4 are obtained that result in the stator current shown as solid (green) line. Finally, the (modified) pattern that falls within the first sampling interval T_s —shown in red in Fig. 5—is applied to the inverter and the horizon is shifted by one T_s .

IV. PERFORMANCE EVALUATION

In this section, the performance of the proposed GP³C scheme for the drive shown in Fig. 1 is assessed using simulations. It is assumed that the IM has a constant mechanical load. The rated values of the MV drive system along with its parameters are provided in Table I. Note that for the given parameters, a total leakage reactance $X_\sigma = 0.255$ p.u. results. The dc-link voltage of the inverter is assumed to be constant. The sampling interval is $T_s = 50 \mu\text{s}$ and a 16-step prediction horizon (i.e., $N_p = 16$) is chosen. The weighting factors are $\lambda_t = 5 \cdot 10^5$ and $\lambda_n = 5$. The OPP in use has pulse number $d = 5$, i.e., the device switching frequency is 250 Hz for operation at nominal speed, while the modulation index is $m = 1.046$. Finally, all results are shown in the p.u. system.

A. Steady-State Performance

The steady-state performance of the MV drive system is examined for operation at nominal speed and rated torque. The corresponding results are presented in Fig. 6. Fig. 6(a) depicts the three-phase stator current over one fundamental period. As can be seen, the current reference tracking capability of the controller is excellent, with only minute deviations from the optimal current trajectory. As a result, the harmonic energy is very low, as indicated by the current TDD I_{TDD} of 4.14%. Furthermore, the harmonic energy is concentrated at frequencies that are odd, non-triplen integer multiples of the fundamental. This is thanks to the symmetry properties of the nominal OPP, which are preserved—to some extent—by the controller, as can be in Fig. 6(c) where the three-phase switching pattern generated by the controller is shown. Additionally, the electromagnetic torque also accurately tracks its reference, see Fig. 6(d), due to the good current reference tracking. Finally, Fig. 6(e), shows that the controller successfully balances the NP potential around its reference, highlighting its multiple-input multiple-output (MIMO) feature and high versatility.

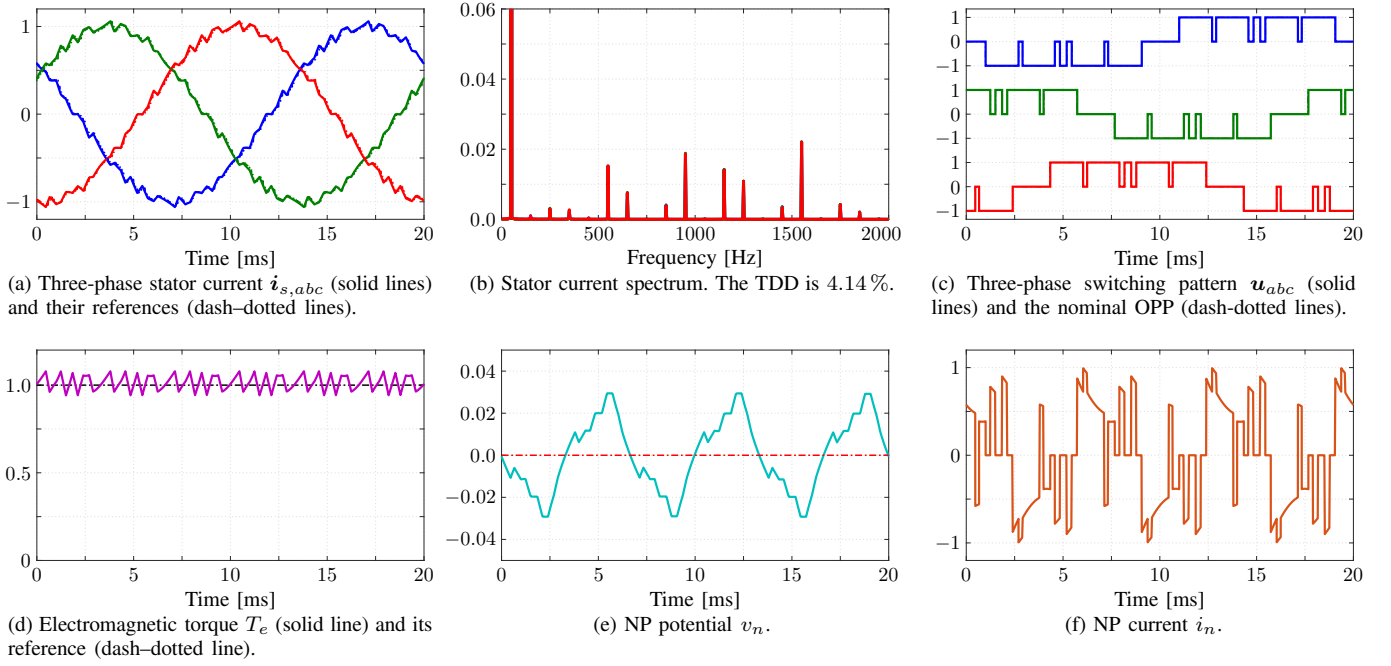


Fig. 6: Simulation results of the proposed GP³C algorithm at steady-state operation, nominal speed and rated torque. The modulation index is $m = 1.046$, the pulse number $d = 5$, and the switching frequency is 250 Hz.

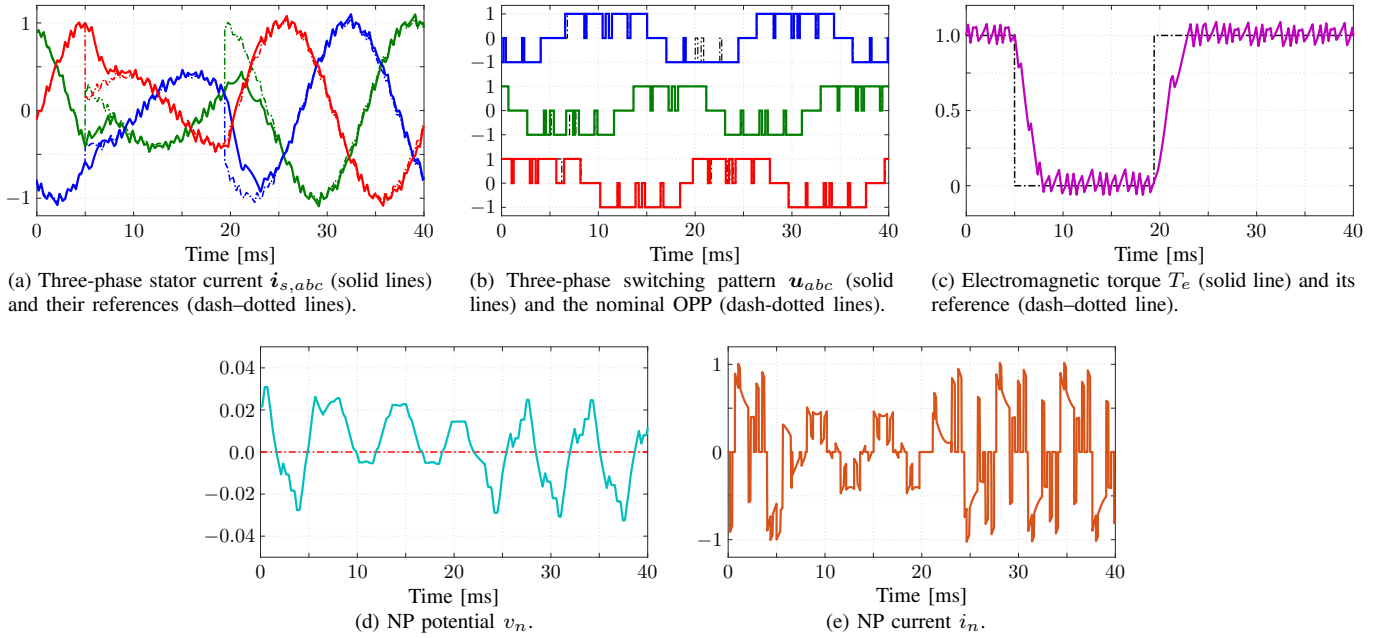


Fig. 7: Simulation results produced by the proposed GP³C algorithm during torque reference steps.

B. Transient Performance

The transient performance of the proposed GP³C scheme is presented in Fig. 7. While operating at nominal speed, reference torque steps of magnitude 1 p.u. are imposed. As can be seen in Fig. 7(a), the stator currents accurately track their new reference values, resulting in an excellent torque reference tracking, see Fig. 7(c). Despite the big changes in the torque reference, GP³C manages to quickly settle to the new operating points by significantly modifying the nominal OPP, see Fig. 8. Specifically, during the torque reference step-down change, the proposed controller modifies the nominal

OPP such that the load angle decreases as fast as possible. As shown in Fig. 8(b), this is done by significantly reducing the width of the pulses in phase c and by shifting forward in time the pulses in phases a and b . Same observations can be made for the step-up case, as illustrated in more detail in Fig. 8(e). It is worth noting that in the latter case, GP³C removes switching pulses from phase a , allowing the available dc-link voltage to be fully utilized. Finally, Fig. 7(d) shows that the NP potential is kept balanced around zero, despite the large changes in the torque as well as operation at zero torque. With regards to the latter, as mentioned, balancing the NP potential at zero torque

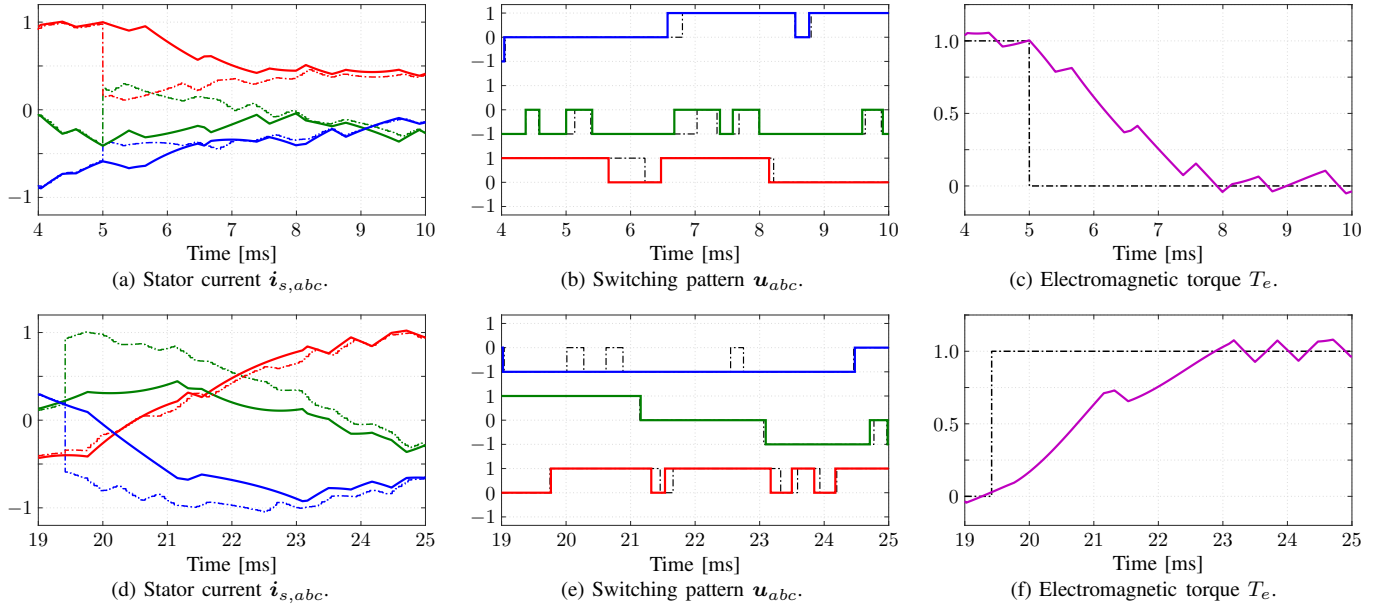


Fig. 8: Transient performance of GP³C at rated speed during a torque reference (a)–(c) step-down change, and (d)–(f) step-up change. In (b) and (e), the (black) dash-dotted lines refer to the switching sequence of the unmodified, nominal OPP, whereas the solid lines correspond to the modified switching sequence as computed by GP³C.

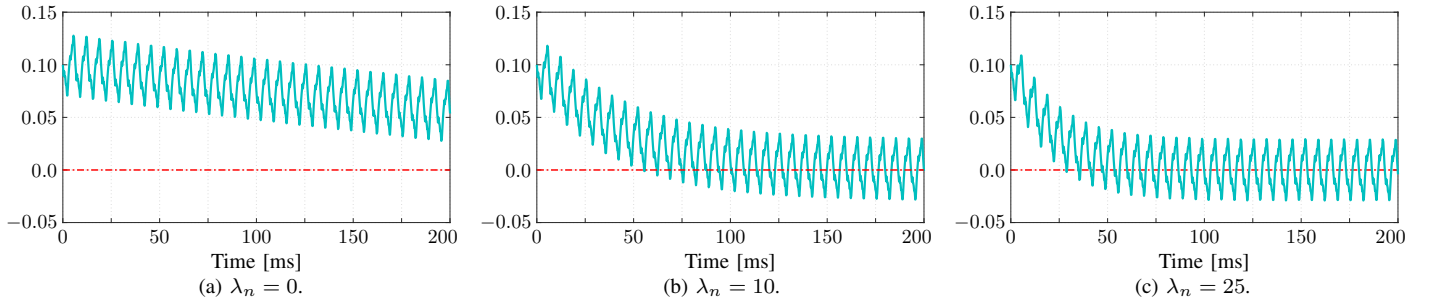


Fig. 9: Balancing of the NP potential for different values of λ_n . The initial offset of the NP potential is 0.1 p.u..

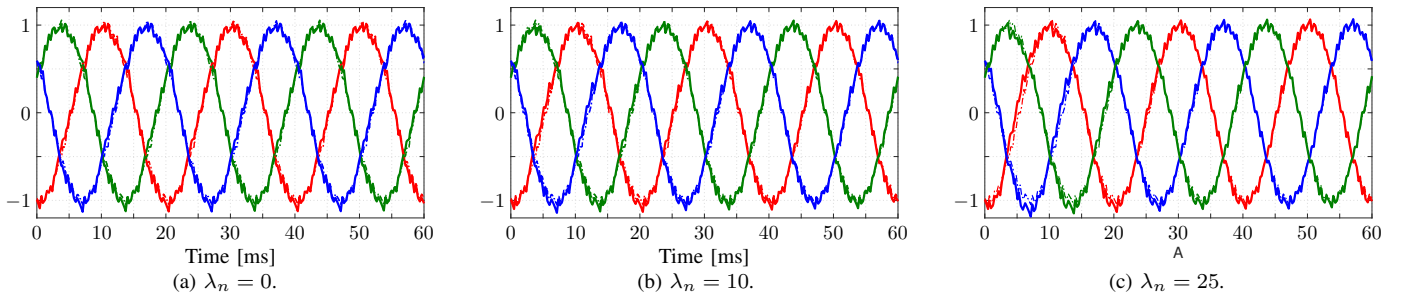


Fig. 10: Three-phase stator current $i_{s,abc}$ when balancing the NP potential for different values of λ_n .

is challenging because the vectors (in the $\alpha\beta$ -frame) of the applied voltage and stator current are perpendicular. Hence, this figure clearly demonstrates the effectiveness of the active balancing mechanism of the proposed control method.

C. Evaluation of the Active NP Potential Balancing Mechanism

Finally, to further investigate the NP potential balancing ability of the proposed algorithm, the weighting factor λ_n is varied and the resulting performance is shown in Fig. 9. For the

presented results operation at nominal speed and rated torque is considered. As can be inferred, the natural balancing of the NP potential, i.e., when $\lambda_n = 0$ (see Fig. 9(a)), is significantly slower compared with the active NP balancing achieved with the proposed controller, i.e., when $\lambda_n > 0$. Specifically, as the controller prioritizes the NP potential balancing, i.e., as λ_n increases, the NP potential is balanced faster, see Figs. 9(b) and 9(c). Additionally, as can be observed in Fig. 10, larger values of λ_n result in a faster regulation of the stator current along its reference. This is facilitated by the fast balancing of the NP potential.

V. CONCLUSIONS

This paper refined the GP³C algorithm introduced in [9] to incorporate the balancing of the NP potential of a three-level NPC inverter into the control problem. The mathematical model adopted within the framework of the proposed controller demonstrates the high versatility of GP³C as well as its ability to simultaneously address multiple control objectives. As highlighted by the presented results, thanks to the combination of optimal constrained control and optimal modulation, the proposed strategy exhibits superior performance during steady state, i.e., minimal current TDD for a given switching frequency, short settling times during transients, and balanced NP potential over the whole operating regime.

APPENDIX A SYSTEM MATRICES

The matrices of the continuous-time state-space model in (7) are

$$F(t) = \begin{bmatrix} F_{IM} & \begin{bmatrix} -\frac{X_r}{D} K |u_{abc}(t)| \\ \mathbf{0}_{2 \times 1} \end{bmatrix} \\ \begin{bmatrix} \frac{1}{2X_{dc}} |u_{abc}(t)|^T K^{-1} & \mathbf{0}_{1 \times 2} \end{bmatrix} & 0 \end{bmatrix},$$

$$G = \frac{v_{dc}}{2} \frac{X_r}{D} \begin{bmatrix} 1 & 0 \\ 0 & 1 \\ 0 & 0 \\ 0 & 0 \\ 0 & 0 \end{bmatrix}, \quad K, \quad C = \begin{bmatrix} 1 & 0 & 0 & 0 & 0 \\ 0 & 1 & 0 & 0 & 0 \\ 0 & 0 & 0 & 0 & 1 \end{bmatrix},$$

where

$$F_{IM} = \begin{bmatrix} -\frac{1}{\tau_s} & 0 & \frac{X_m}{\tau_r D} & \omega_r \frac{X_m}{D} \\ 0 & -\frac{1}{\tau_s} & -\omega_r \frac{X_m}{D} & \frac{X_m}{\tau_r D} \\ \frac{X_m}{\tau_r} & 0 & -\frac{1}{\tau_r} & -\omega_r \\ 0 & \frac{X_m}{\tau_r} & \omega_r & -\frac{1}{\tau_r} \end{bmatrix}.$$

APPENDIX B OBJECTIVE FUNCTION MATRICES

The vector \mathbf{r} and matrix \mathbf{M} in (13) are

$$\mathbf{r} = \begin{bmatrix} \mathbf{y}_{ref}(t_{1,ref}) - \mathbf{y}(t_0) \\ \mathbf{y}_{ref}(t_{2,ref}) - \mathbf{y}(t_0) \\ \mathbf{y}_{ref}(t_{3,ref}) - \mathbf{y}(t_0) \\ \vdots \\ \mathbf{y}_{ref}(t_{z,ref}) - \mathbf{y}(t_0) \end{bmatrix}$$

and

$$\mathbf{M} = \begin{bmatrix} \mathbf{m}_{t_0} & \mathbf{0}_2 & \mathbf{0}_2 & \dots & \mathbf{0}_2 \\ \mathbf{m}_0 & \mathbf{m}_{t_1} & \mathbf{0}_2 & \dots & \mathbf{0}_2 \\ \mathbf{m}_0 & \mathbf{m}_1 & \mathbf{m}_{t_2} & \dots & \mathbf{0}_2 \\ \vdots & \vdots & \vdots & \ddots & \vdots \\ \mathbf{m}_0 & \mathbf{m}_1 & \mathbf{m}_2 & \dots & \mathbf{0}_2 \\ \mathbf{m}_0 & \mathbf{m}_1 & \mathbf{m}_2 & \dots & \mathbf{m}_{t_{z-1}} \end{bmatrix}$$

with

$$\mathbf{m}_{t_\ell} = \mathbf{m}(t_{\ell,ref})$$

$$\mathbf{m}_\ell = \mathbf{m}(t_{\ell,ref}) - \mathbf{m}(t_{\ell+1,ref})$$

where $\ell \in \{0, 1, 2, \dots, z-1\}$.

REFERENCES

- [1] A. K. Rathore, J. Holtz, and T. Boller, "Synchronous optimal pulsewidth modulation for low-switching-frequency control of medium-voltage multilevel inverters," *IEEE Trans. Ind. Electron.*, vol. 57, no. 7, pp. 2374–2381, Jul. 2010.
- [2] G. S. Buja, "Optimum output waveforms in PWM inverters," *IEEE Trans. Ind. Appl.*, vol. IA-16, no. 6, pp. 830–836, Nov./Dec. 1980.
- [3] J. Holtz and B. Beyer, "Optimal synchronous pulsewidth modulation with a trajectory-tracking scheme for high-dynamic performance," *IEEE Trans. Ind. Appl.*, vol. 29, no. 6, pp. 1098–1105, Nov./Dec. 1993.
- [4] —, "The trajectory tracking approach—a new method for minimum distortion PWM in dynamic high-power drives," *IEEE Trans. Ind. Appl.*, vol. 30, no. 4, pp. 1048–1057, Aug. 1994.
- [5] J. Holtz and N. Oikonomou, "Synchronous optimal pulsewidth modulation and stator flux trajectory control for medium-voltage drives," *IEEE Trans. Ind. Appl.*, vol. 43, no. 2, pp. 600–608, Mar./Apr. 2007.
- [6] T. Geyer, N. Oikonomou, G. Papafotiou, and F. D. Kieferndorf, "Model predictive pulse pattern control," *IEEE Trans. Ind. Appl.*, vol. 48, no. 2, pp. 663–676, Mar./Apr. 2012.
- [7] N. Oikonomou, C. Gutscher, P. Karamanakos, F. D. Kieferndorf, and T. Geyer, "Model predictive pulse pattern control for the five-level active neutral-point-clamped inverter," *IEEE Trans. Ind. Appl.*, vol. 49, no. 6, pp. 2583–2592, Nov./Dec. 2013.
- [8] T. Geyer, V. Spudić, W. van der Merwe, and E. Guidi, "Model predictive pulse pattern control of medium-voltage neutral-point-clamped inverter drives," in *Proc. IEEE Energy Convers. Congr. Expo.*, Portland, OR, USA, Sep. 2018, pp. 5047–5054.
- [9] M. A. W. Begh, P. Karamanakos, and T. Geyer, "Gradient-based predictive pulse pattern control," in *Proc. IEEE Energy Convers. Congr. Expo.*, Vancouver, BC, Canada, Oct. 2021, pp. 4682–4689.
- [10] H. du Toit Mouton, "Natural balancing of three-level neutral-point-clamped pwm inverters," *IEEE Trans. Ind. Electron.*, vol. 49, no. 5, pp. 1017–1025, Oct. 2002.
- [11] J. K. Steinke, "Switching frequency optimal PWM control of a three-level inverter," *IEEE Trans. Power Electron.*, vol. 7, no. 3, pp. 487–496, Jul. 1992.
- [12] S. Ogasawara and H. Akagi, "Analysis of variation of neutral point potential in neutral-point-clamped voltage source PWM inverters," in *Proc. IEEE Ind. App. Soc. Annu. Mtg.*, Toronto, ON, Canada, Oct. 1993, pp. 965–970.
- [13] C. Newton and M. Sumner, "Neutral point control for multi-level inverters: Theory, design and operational limitations," in *Proc. IEEE Ind. App. Soc. Annu. Mtg.*, New Orleans, LA, Oct. 1997, pp. 1336–1343.
- [14] J. Pou, R. Pindado, D. Boroyevich, and P. Rodríguez, "Evaluation of the low-frequency neutral-point voltage oscillations in the three-level inverter," *IEEE Trans. Ind. Electron.*, vol. 52, no. 6, pp. 1582–1588, Dec. 2005.
- [15] J. Holtz and N. Oikonomou, "Neutral point potential balancing algorithm at low modulation index for three-level inverter medium-voltage drives," *IEEE Trans. Ind. Appl.*, vol. 43, no. 3, pp. 761–768, May 2007.
- [16] T. Boller, J. Holtz, and A. K. Rathore, "Neutral-point potential balancing using synchronous optimal pulsewidth modulation of multilevel inverters in medium-voltage high-power ac drives," *IEEE Trans. Ind. Appl.*, vol. 50, no. 1, pp. 549–557, Jan./Feb. 2014.
- [17] T. Geyer and V. Spudić, "Model predictive pulse pattern control with integrated balancing of the neutral point potential," in *Proc. Eur. Power Electron. Conf.*, Genova, Italy, Nov. 2019, pp. 1–10.
- [18] T. Geyer, *Model Predictive Control of High Power Converters and Industrial Drives*. Hoboken, NJ, USA: Wiley, 2016.
- [19] J. Holtz, "The representation of ac machine dynamics by complex signal flow graphs," *IEEE Trans. Ind. Electron.*, vol. 42, no. 3, pp. 263–271, Jun. 1995.
- [20] G. S. Buja and G. B. Indri, "Optimal pulsewidth modulation for feeding ac motors," *IEEE Trans. Ind. Appl.*, vol. IA-13, no. 1, pp. 38–44, Jan. 1977.
- [21] P. Karamanakos, R. Mattila, and T. Geyer, "Fixed switching frequency direct model predictive control based on output current gradients," in *Proc. IEEE Ind. Electron. Conf.*, Washington, D.C., USA, Oct. 2018, pp. 2329–2334.
- [22] P. Karamanakos, M. Nahalparvari, and T. Geyer, "Fixed switching frequency direct model predictive control with continuous and discontinuous modulation for grid-tied converters with *LCL* filters," *IEEE Trans. Control Sys. Technol.*, vol. 29, no. 4, pp. 1503–1518, Jul. 2021.